*Proceedings of the 20th International Conference on Soil Mechanics and Geotechnical Engineering– Rahman and Jaksa (Eds)*


# Combined effects of scour and earthquake on lateral responses of piles in sands

## Effets combinés de l'affouillement et du séisme sur les réponses latérales des pieux dans les sables

**Cheng Lin** & Wenyu Jiang
*Department of Civil Engineering, University of Victoria, Canada, chenglin918@uvic.ca*

ABSTRACT: Scour-induced soil loss can significantly change the lateral responses of the pile-supported structures under the imposed seismic demands. However, the combined effects of scour and earthquake on the dynamic responses of piles are in general not fully appreciated. The current design manuals including those from the US Federal Highway Administration (FHWA) and American Petroleum Institute (API) recommended different methods to evaluate the lateral responses of piles under prescribed scour-hole conditions, which thus lead to different seismic designs. The objective of this paper is to examine the suitability of these standard methods for the evaluation of the combined effects of scour and earthquake by comparing them to an analytical solution. Using the developed computer scripts following the standard methods and the analytical solution, a series of parametric analyses was conducted for piles in sands subjected to both scour and earthquake. Based on the comparative analyses, recommendations were developed for selecting an appropriate method to conduct seismic designs of piles under different scour-hole dimensions.

RÉSUMÉ : La perte de sol induite par l'affouillement peut modifier considérablement les réponses latérales des structures sur pieux sous les exigences sismiques imposées. Cependant, les effets combinés de l'affouillement et du séisme sur les réponses dynamiques des pieux ne sont généralement pas totalement appréciés. Les manuels de conception existants, y compris ceux de la Federal Highway Administration (FHWA) des États-Unis et de l'American Petroleum Institute (API), recommandaient différentes méthodes pour évaluer les réponses latérales des pieux dans les conditions de fosse d'affouillement prescrites, ce qui conduit à des conceptions sismiques différentes. L'objectif de cet article est d'examiner la pertinence de ces méthodes standard pour l'évaluation des effets combinés de l'affouillement et du séisme en les comparant à une solution analytique. En utilisant les scripts informatiques développés suivant les méthodes standard et la solution analytique, une série d'analyses paramétriques a été réalisée pour les pieux dans les sables soumis à la fois à l'affouillement et au séisme. Sur la base des analyses comparatives, des recommandations ont été formulées pour sélectionner une méthode appropriée pour réaliser des conceptions sismiques de pieux sous différentes dimensions de fosse d'affouillement.

KEYWORDS: Earthquake, local scour, pile, scour-hole dimensions, sand.

## 1 INTRODUCTION

For structures in waters, scour can be a major hazard that threatens their serviceability and safety. Typically, scour at a foundation supporting the structure includes general scour that uniformly lowers mudline elevation, and local scour that forms a localized pit around the foundation. For deep foundations, by removing soils around piles, scour results in a decrease in pile capacities and changes in dynamic responses of the integrated soil-pile-superstructure system. At present, most of the relevant studies (Wang et al. 2015, Jia et al. 2017, Jiang and Lin 2020) are focused on seismic responses of piles under general scour; however, only limited studies (Liang et al. 2020, Zhu et al. 2020) are focused on the seismic responses of piles under local scour, in which centrifuge model tests are utilized for the investigation. Moreover, a proper method capable of considering the combined effects of scour and earthquake on piles has not been formulated for practical design purposes. Therefore, it is worthwhile to propose a practical method for analyzing the post-scour dynamic responses of piles considering various scour-hole dimensions.

In general, dynamic responses of piles are analyzed using a dynamic-beam-on-nonlinear-Winkler-foundation (DBNWF) approach (Boulanger et al. 1999), in which soil-pile interactions are represented by *p-y*, *t-z*, and *q-z* springs in parallel with dashpots. According to Jiang et al. (2021), the post-scour dynamic responses of piles under local scour can be evaluated by modifying these springs through incorporating the decrease in soil overburden induced by local scour into equations of ultimate soil resistances to piles. The scour-induced decrease in soil stress or post-scour soil stress at piles can be estimated in prevailing design manuals, including American Petroleum Institute (dubbed as API) (API 2011), US Federal Highway Administration-Driven Piles (dubbed as FHWA-DP) (Patrick et al. 2016) and FHWA-Drilled shafts (dubbed as FHWA-DS) (Brown et al. 2010). However, these standard methods suggest different ways for the estimation and are only applicable for a limited range of scour-hole dimensions that are not adequate to reflect those observed in field (Butch 1996). Consequently, the authors (Lin and Wu 2019, Lin and Jiang 2019) proposed an analytical solution to compute the post-scour vertical effective stress at a single pile to accommodate for various scour-hole dimensions. Although the analytical solution and the standard methods are critically assessed for scoured piles under static loading (Lin and Wu 2019, Lin and Jiang 2019, Lin and Lin 2019), they have not been compared and evaluated in the dynamic analysis. Therefore, the suitability of these standard methods for analyzing combined effects of scour and earthquake is not fully appreciated.

The objectives of this study are twofold. Firstly, we developed two types of modified DBNWF numerical models to consider the effects of different scour-hole dimensions and earthquake ground motions using the proposed analytical solution and the standard methods (i.e., API, FHWA-DP, and FHWA-DS) for piles in liquefiable sands. The analytical solution was validated against a centrifuge test in the literature. Secondly, a series of 29 parametric analyses were performed using the numerical models to elucidate the effects of scour-hole depth on the lateral responses of scoured piles under a selected crustal earthquake. Based on the results of the parametric study, the standard methods were critically assessed for their suitability for the evaluation of the combined effects of scour and earthquake on piles.

## 2 METHODS FOR EVALUATION OF VERTICAL EFFECTIVE STRESS UNDER LOCAL SCOUR

In the routine design of pile foundations, the vertical effective soil stress at pile is calculated prior to the evaluation of lateral and vertical pile capacities. Therefore, an appropriate calculation of post-scour vertical effective stress is the key to determine the pile behavior affected by local scour. Typically, a local-scour hole can be simplified as an inverted truncated cone characterized by scour-hole depth ($S_d$), bottom width ($S_w$), and side slope angle ($S_\theta$) (Figure 1). Affected by local scour, the vertical effective stress (or soil overburden) is decreased. But the stress reduction only occurs within a certain depth, termed as an influence depth, beyond which the stress remains unchanged by the local scour. This section summarizes two sets of practical approaches for calculating the vertical effective stress considering scour-hole dimensions.

### 2.1 *Standard methods*

The post-scour vertical effective stress ($\sigma'_{v,sc}$) per the standard methods is mathematically written in Eq. 1.

$$\sigma'_{v,sc} = \begin{cases} \gamma' z(1 + S_d/z_i) & \text{for } z < z_i \\ \gamma'(S_d + z) & \text{for } z \geq z_i \end{cases} \quad (1)$$

where $\gamma'$ = effective unit weight of soil; $z$ = depth below the scour-hole bottom; $S_d$ = scour-hole depth; $z_i$ = influence depth. Figure 1 shows the depth distribution of post-scour vertical effective stress following different design standards. As shown, FHWA-DP ignores the scour-induced reduction in the vertical effective stress, and therefore, the depth-distribution of post-scour vertical effective stress follows that of pre-scour vertical effective stress (i.e., $z_i = 0$). Contrarily, both API and FHWA-DS acknowledge the scour-induced stress reduction for soils at depths less than $z_i$ but no reduction at depths greater than $z_i$. However, FHWA-DS recommends $z_i = 1.5S_d$ for various $S_d$ while $S_w = 0$ and $S_\theta = 26.6°$; API recommends the stress reduction be extended to a depth of $6D$ ($D$ = pile diameter) with respect to the pre-scour ground surface for a typical scour-hole depth $S_d = 1.5D$ and $S_w = 0$ but gives no recommendations to $S_\theta$. This may be interpreted as the influence depth $z_i = 3S_d$, while $S_\theta = 30°$ may be used in marine foundations (Whitehouse 1998). In the parametric study, the standard methods only differed in $z_i$ for various $S_d$ but assumed the same values for $S_w$ and $S_\theta$ ($S_w = 0$ and $S_\theta = 30°$) for comparison purposes.

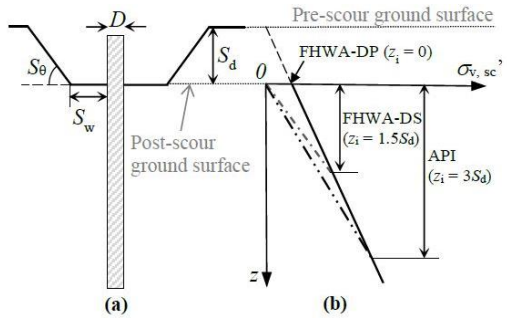


Figure 1. (a) Scour-hole dimensions and (b) vertical effective stress distribution per standard methods (API, FHWA-DP, and FHWA-DS).

### 2.2 *Analytical solution*

Since the standard methods are largely empirical and only applicable for limited scour-hole dimensions, an analytical solution that accounts for different scour-hole dimensions was proposed (Lin and Wu 2019, Lin and Jiang 2019), as expressed by Eq. 2, in which the post-scour vertical effective stress ($\sigma'_{v,sc}$) is calculated by superposition of two components of vertical effective stress resulting from soil overburden below and above the post-scour ground surface. The former is simply calculated as $\gamma' z$, while the latter that accounts for various scour-hole dimensions is derived from the Boussinesq point load solution.

$$\sigma'_{v,sc} = \gamma' z \left[1 + \left(\frac{S_d/\tan S_\theta + S_w}{\sqrt{(S_d/\tan S_\theta + S_w)^2 + z^2}} - \frac{S_w}{\sqrt{S_w^2 + z^2}}\right)\tan S_\theta\right] \quad (2)$$

Once the post-scour vertical effective stress ($\sigma'_{v,sc}$ invoking Eq. 1 for the standard methods but Eq. 2 for the analytical solution) is calculated, the conventional sand *p-y* (API 2011), *t-z* (Mosher 1984), and *q-z* (Vijayvergiya 1977) curves can be practically modified to account for scour-hole dimensions and liquefaction-induced softening of soils, as will be discussed in Section 3.2.

## 3 DEVELOPMENT OF NUMERICAL MODEL

To analyze the dynamic responses of piles in liquefiable sands under the combined effects of local scour and earthquake loading, this study developed a modified dynamic-beam-on-nonlinear-Winkler-foundation (DBNWF) model via an open-source platform OpenSees (McKenna 2011). As shown in Figure 2, the integrated finite element (FE) model includes a free-field soil column to capture the upward propagation of seismic waves, a pile modeled by displacement-based nonlinear beam elements, and spring-dashpot elements to capture soil-pile interactions considering scour-hole dimensions and liquefaction-induced softening. Besides, a mass block was attached to the pile top to render a similar natural frequency to a soil-pile-superstructure system (Zhu et al. 2020). The energy dissipation was simulated by Raleigh damping, and a total damping ratio of 3% (Bhattacharya 2019) was assigned to the integrated system accounting for its first and second modes of natural frequencies (Mo et al. 2017).

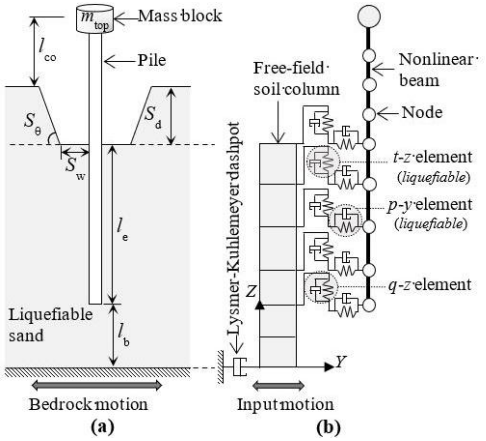


Figure 2. Illustrations of (a) physical model and (b) FE model for a pile in liquefiable sands under local scour and earthquake.

### 3.1 *Free-field soil column for effective stress analysis*

To capture the liquefaction-induced softening of saturated sands under strong ground motions, free-field motions were computed based on effective stress analysis. As will be discussed in Section 3.2, the computed excess pore water pressure and effective stress in the free-field soils would be further used to construct liquefiable *p-y*, *t-z*, and *q-z* curves following the method by Brandenberg et al. (2013). The pressure-dependent multi-yield material was embedded in the fluid-solid porous material (Yang et al. 2003) for simulating the saturated sands, and the out-of-plane thickness of the free-field soil column was set to be 500 m to preclude the influence of soil-pile interaction (Khosravifar et al. 2014).

As shown in Figure 2, a dashpot per Lysmer and Kuhlemeyer (1969) was introduced at the base of the free-field column to account for the finite rigidity of the underlying half-space. Correspondingly, earthquake loading was applied as a time history of force to the free-field base (Joyner and Chen 1975). The time history of force is the product of the dashpot coefficient ($c_b$ in Eq. 3) and the time history of velocity recorded on a rock outcrop or firm ground (i.e., outcropping motion).

$$c_b = A_b \rho_b V_b \tag{3}$$

where $A_b$ = cross-section area of free-field column; $\rho_b$ = mass density of bedrock/firm soils, taken as 2.2 ton/m$^3$ (Uthayakumar and Naesgaard 2004); $V_b$ = shear wave velocity of bedrock/firm soils, taken as 760 m/s (NRCC 2015). Alternatively, if the selected earthquake motions were recorded on the embedded bedrock/firm soils (i.e., within motion), a rigid bedrock condition would be adopted by removing the dashpot from the base of the free-field column; correspondingly, the recorded acceleration time history would be applied to the free-field base according to the uniform excitation method (McKenna 2011).

### 3.2 *Soil-pile interaction under local scour*

The soil-pile interactions in liquefiable sands are simulated by the modified *p-y* (API 2011), *t-z* (Mosher 1984), and *q-z* (Vijayvergiya 1977) springs in parallel with linear dashpots.

#### 3.2.1 *Horizontal springs and dashpots*

API sand *p-y* curve is primarily dependent on the ultimate lateral soil resistance and initial modulus of subgrade reaction ($k$). Since the scour effect on $k$ was found to be negligible (Lin and Lin 2019), the post-scour *p-y* relation can be developed by using the ultimate soil resistance considering scour-hole dimensions.

$$p = 0.9 p_{u,sc} \tanh\left(\frac{k y \sigma'_{v,sc}}{0.9 \gamma' p_{u,sc}}\right) \tag{4}$$

$$p_{u,sc} = \min\left[\left(\frac{c_1 \sigma'_{v,sc}}{\gamma'} + c_2 D\right)\sigma'_{v,sc}, c_3 D \sigma'_{v,sc}\right] \tag{5}$$

where $p_{u,sc}$ = ultimate lateral resistance under local scour condition; $\sigma'_{v,sc}$ is computed using Eq. 1 (standard methods) or Eq. 2 (analytical solution). The coefficients ($c_1 - c_3$) and $k$ are dependent on the internal friction angle of soil ($\phi'$) (API 2011). Subsequently, by substituting $p_{u,sc}$ into *PyLiq1* material in OpenSees, the post-scour *p-y* curve can be further scaled in proportion to the mean effective stress within two adjacent free-field soil elements to capture the softening effect due to the increased excess pore water pressure. The residual ultimate soil resistance when the soil element fully liquefies was taken as $0.1 p_{u,sc}$ (Lombardi and Bhattacharya 2016). Readers should refer to Brandenberg et al. (2013) for more details on the liquefiable spring material. Besides, radiation damping under earthquake loading was simulated by a linear dashpot. Based on Wang et al. (1998) and Khosravifar et al. (2014), the damping coefficient of the horizontal dashpot ($c_h$) was taken as

$$c_h = 4 D \rho V_s \Delta z \tag{6}$$

where $\rho$ = saturated mass density of soil; $\Delta z$ = tributary size of spring; $V_s$ = shear wave velocity of soil. Note that $V_s$ was taken as 10% of the pre-earthquake value to consider the liquefaction-induced softening of soils (Khosravifar et al. 2014).

#### 3.2.2 *Vertical springs and dashpots*

Likewise, *t-z* (Mosher 1984) and *q-z* (Vijayvergiya 1977) springs were modified to account for the effects of local scour and liquefaction-induced softening.

$$t = \left[\gamma' / (\sigma'_{v,sc} E_f) + t_{u,sc}{}^{-1}\right]^{-1} \tag{7}$$

$$t_{u,sc} = \beta \sigma'_{v,sc} \tag{8}$$

where $E_f$ = initial modulus of soil, which can be correlated to $\phi'$ (Mosher 1984); $t_{u,sc}$ = ultimate shaft friction under local scour condition; $\beta$ = dimensionless shaft friction factor dependent on the relative density of sands ($D_r$) (API 2011). As with the foregoing procedure for considering the liquefaction-induced softening, we substituted $t_{u,sc}$ into *TzLiq1* material in OpenSees with a residual peak value of $0.1 t_{u,sc}$. The radiation damping coefficient ($c_v$) per George and Dobry (1984) is written in Eq. 9, where $V_s$ was taken as 10% of the pre-earthquake value.

$$c_v = 2\pi D \rho V_s \Delta z \tag{9}$$

Besides, Vijayvergiya's *q-z* relation was modified as

$$q = N_q \sigma'_{v,sc}\left[\sigma'_{v,sc} / (\gamma' z_c)\right]^{1/3} \tag{10}$$

where $z_c$ = critical displacement taken as $0.05D$ (Vijayvergiya 1977); $N_q$ = end bearing factor dependent on $D_r$ (API 2011). The *q-z* spring was simulated using *QzSimple1* material in OpenSees since the excess pore water pressure is typically negligible in the end bearing stratum (Brandenberg et al. 2013). Consequently, the radiation damping coefficient was calculated using Eq. 9 but without a reduction in $V_s$.

### 3.3 *Validation of analytical solution*

The DBNWF method for the evaluation of pile dynamic responses has been extensively validated by comparing the numerical results with both centrifuge tests (Boulanger et al. 1999, Ilankatharan 2008) and three-dimensional sophisticated numerical models (Kampitsis et al. 2013). The liquefiable soil springs and free-field soil materials were also verified against centrifuge tests (Yang et al. 2003, Brandenberg et al. 2013).

Here, we were to validate the modified DBNWF model using the proposed analytical solution for scoured piles under earthquake loading. The centrifuge test (Zhu et al. 2020) of fixed-end piles in medium sands under combined effects of dynamic excitation and local scour ($S_d = 2D$, $S_w = D$, and $S_\theta = 30°$) was referenced to validate the computed fundamental frequency and pile-top response acceleration. The parameters of the pipe pile are listed in Table 1. The soil used was Fujian standard sand ($D_r = 60\%$, $\phi' = 40°$, and $\gamma' = 9.36$ kN/m$^3$). The shear wave velocity ($V_s$) and small-strain shear modulus ($G_{max}$) (Seed et al. 1986) were calculated as

$$V_s = \sqrt{G_{max}/\rho} \tag{11}$$

$$G_{max} = 1000 K_{2,max} \sqrt{\sigma'_m} \tag{12}$$

where $\sigma'_m$ = mean effective stress; $K_{2,max}$ = dimensionless factor estimated based on $D_r$ (Seed et al. 1986), taken as 52 herein. Note that the units of $\sigma'_m$ and $G_{max}$ are lb/ft$^2$ in Eq. 12. The soil parameters used for the free-field soils were taken as the suggested values for medium sands (Yang et al. 2003).

Table 1. Pile parameters extracted from Zhu et al. (2020).

| Property | $D$ (m) | $t$ (m) | $R_p$ (MN·m$^2$) | $l_{eo}$ (m) | $l_{co}$ (m) | $\sigma_y$ (MPa) | $m_{top}$ (ton) |
|---|---|---|---|---|---|---|---|
| Value | 1.5 | 0.02 | 5300 | 20 | 32 | 290 | 100 |

Note: $t$ = wall thickness; $R_p$ = flexural rigidity; $\sigma_y$ = yielding stress; $l_{eo}$ and $l_{co}$ = pre-scour embedment length ($l_{eo} = l_e + S_d$) and unsupported length, respectively.

As shown in Table 2, post-scour fundamental frequency ($f_0$) of the integrated system computed by the developed script using

the analytical solution (dubbed as FEM) agrees well with the measured value. As with Tseng et al. (2018), the DBNWF model could render reasonable estimations of natural frequency.

Table 2. Fundamental frequencies before and after scour (test vs. FEM).

| Source | Pre-scour (Hz) | Post-scour (Hz) | Percentage change (%) |
|---|---|---|---|
| Test | 0.268 | 0.230 | 14 |
| FEM | 0.268 | 0.237 | 12 |

Furthermore, pile-top accelerations under three input motions were computed by the FEM and compared with the measured responses (Figure 3). The input motions with different peak accelerations ($a_{max}$) of 0.1g, 0.2g, and 0.4g were applied to the rigid base of the model box in tests (i.e., within motions on a rigid bedrock in FEM). As shown, the computed acceleration responses from the FEM agree reasonably with the centrifuge tests before and after scour. Overall, credence is given to the developed pre-scour FE model and the post-scour FE model following the proposed analytical solution.

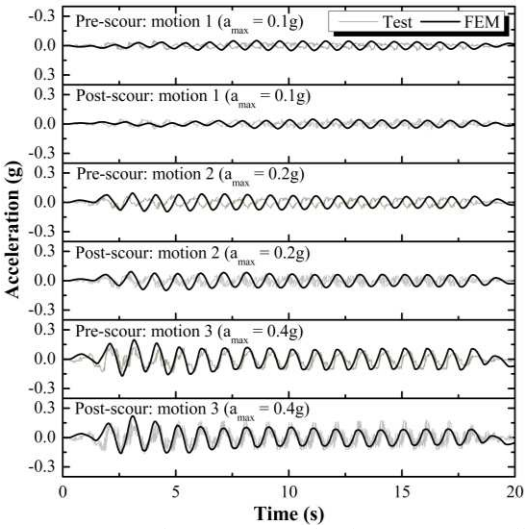


Figure 3. Pre-scour and post-scour acceleration responses at pile top under three input motions (centrifuge test vs. FEM).

## 4 PARAMETRIC ANALYSES

The monopile for small megawatt offshore wind turbines from Zhu et al. (2020) was selected for the parametric study with a modification of the pile-tip boundary condition from the fixed pile tip to the pile tip embedded in soils (Figure 2). The parameters of pile and soil are provided in Section 3.3. The soil thickness from the bedrock to the initial (pre-scour) seabed was taken as 30 m (Uthayakumar and Naesgaard 2004). As shown in Figure 4, an outcropping motion from the Loma Prieta earthquake, which was recorded at the bedrock or firm ground corresponding to site class C per NRCC (2015), was selected as the input motion. The peak bedrock acceleration (PBA) was 0.64g, which falls in the range of 0.5g to 0.7g used by previous studies (Chang et al. 2013, Yang et al. 2019).

Because vertical and lateral capacities of the pile under local scour are mainly dependent on the scour-hole depth ($S_d$) (Lin and Jiang 2019, Jiang et al. 2021), numerical analyses were focused on the effect of $S_d$ on the seismic responses of the pile, while the scour-hole bottom width ($S_w$) and side slope angle ($S_\theta$) were taken as $S_w = 0$ and $S_\theta = 30°$, respectively (Jiang et al. 2021). Eight scour-hole depths were considered in the numerical analyses, which included $S_d(\times D) =$ 0, 0.5, 1.0, 1.3, 1.5, 2.0, 2.5, and 3.0. The post-scour embedded length of pile ranged from 10.3$D$ to 12.8$D$ when $S_d$ = 0.5$D$-3.0$D$. The examined range of $S_d$ was selected to cover the typical design values ($S_d$ = 1.3$D$-2.5$D$) (API 2011, GL 2012, DNV 2014). The post-scour cases were analyzed using the analytical solution and standard methods (API, FHWA-DP, and FHWA-DS); therefore, a total of 29 cases were performed in the parametric analyses.

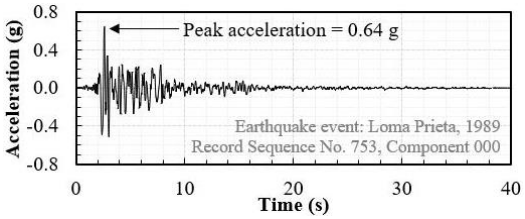


Figure 4. Input motion in time history of acceleration

## 5 RESULTS AND DISCUSSION

The maximum bending moment of the pile and the maximum rotation of the pile at the post-scour seabed level under different scour-hole dimensions are presented, aimed at assessment of different standard methods in analyses of combined effects of scour and earthquake. Besides, the maximum dynamic responses of the pile under different scour-hole dimensions are presented in a normalized way, i.e., the calculated dynamic responses were normalized by the corresponding pre-scour values.

The dynamic responses presented in this paper are the maximum bending moment and rotation of the monopile, which are two parameters of engineering importance in design practice (DNV 2014, Bhattacharya 2019). The normalized maximum bending moment of the pile and the normalized maximum rotation of the pile at the post-scour seabed were obtained following the three steps:

(1) Profile the response envelopes of bending moment (e.g., Figure 5) and rotation, with each value in the envelope taken as the peak value of the time-domain responses at the corresponding elevation of the pile.

(2) Find the maximum bending moment of the pile and the maximum rotation of the pile at the post-scour seabed from the envelopes determined in (1).

(3) Calculate the normalized response by dividing the maximum post-scour response by the corresponding pre-scour maximum response; therefore, the normalized value greater than unity implies the scour-induced amplification in the response, and vice versa.

For demonstration, Figure 5 is presented here to show the envelopes of the bending moment under different $S_d$ computed by the analytical solution.

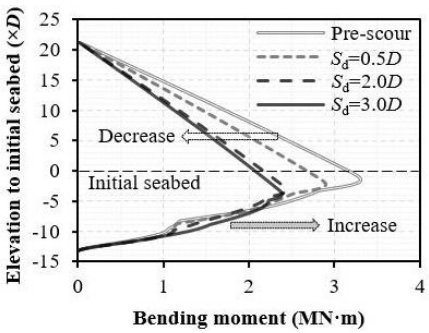


Figure 5. Envelopes of bending moment before and after scour.

As shown in Figure 5, the location corresponding to the maximum bending moment occurred at a depth of 1.5$D$-3.9$D$ below the pre-scour seabed when $S_d$ = 0-3.0$D$. In other words, the location of the maximum bending moment moved downward relative to the pile top but upward relative to the post-scour seabed as $S_d$ increased. Besides, at soil depth greater than 7$D$ below the pre-scour seabed, the envelope of the

bending moment tended to increase as $S_d$ increased. Contrarily, the maximum bending moment of monopile was decreased by scour. For example, the maximum bending moments before and after scour ($S_d = 3.0D$, $S_w = 0$, and $S_\theta = 30°$ ) were 3.3 MN·m and 2.4 MN·m, respectively. Accordingly, the normalized value is 0.72, indicating the maximum bending moment of monopile was decreased by 28% due to scour. The different trend is because the inertial interaction tended to be out-of-phase with the kinematic interaction, resulting in a decrease in the maximum pile stress for a slender superstructure (Tokimatsu et al. 2005).

### 5.1 MAXIMUM BENDING MOMENT VERSUS SCOUR-HOLE DEPTH

Figure 6 shows the normalized maximum bending moment of the pile under different scour-hole depths computed by different methods. As indicated by the analytical solution, the normalized value decreased almost linearly from 1.0 to 0.74 (26% reduction) as $S_d$ increased from 0 to $2.0D$. However, the reduction ceased when $S_d = 2.0D$-$3.0D$. This is because the kinematic interaction prevailed over the inertial interaction at a deeper depth where the maximum bending moment tended to occur as $S_d$ increased (Figure 5).

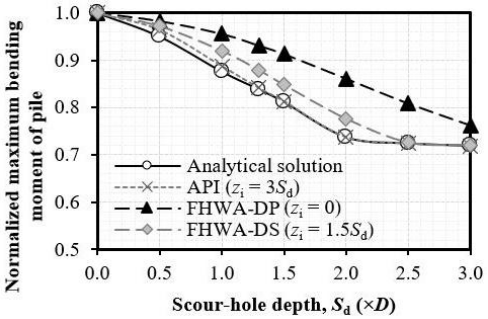


Figure 6. Normalized maximum bending moment of pile varied by scour-hole depths.

In comparison to the analytical solution, FHWA-DS and FHWA-DP were found to overestimate the normalized maximum bending moment by up to 5% and 17%, respectively, while API provided agreeable results when $S_d = 1.3D$-$3.0D$. Overall, as with Ghosn et al. (2003) and Boulanger et al. (1999), the scour-induced decrease in the stiffness of the integrated system could reduce the maximum internal forces of piles. On one end, this indicates scour could be beneficial for a pile in responding to seismic loading. On the other end, however, it implies that employing an overestimated $S_d$ value in the seismic design of piles against scour could potentially underestimate the maximum bending moment and cause an unconservative design.

### 5.2 MAXIMUM ROTATION VERSUS SCOUR-HOLE DEPTH

Figure 7 shows the normalized maximum rotation of pile at the post-scour seabed varied with $S_d$. Unlike the relationship between the maximum bending moment and $S_d$, the maximum rotation at the post-scour seabed increased as $S_d$ increased. Compared with the pre-scour value, the normalized rotation increased by 11%-20% when $S_d = 1.3D$-$2.5D$ as indicated by the analytical solution.

In general, API and FHWA-DS produced similar results with the analytical solution, while FHWA-DP overestimated the maximum rotation of pile at the post-scour seabed by up to 2% compared with the other methods. Since the maximum rotation of the pile at the post-scour seabed is typically specified to be less than 0.5° (DNV 2014, Bhattacharya 2019), it is appropriate to employ a larger value of $S_d$ in the typical range of $1.3D$-$2.5D$ to provide a more conservative evaluation of rotation response.

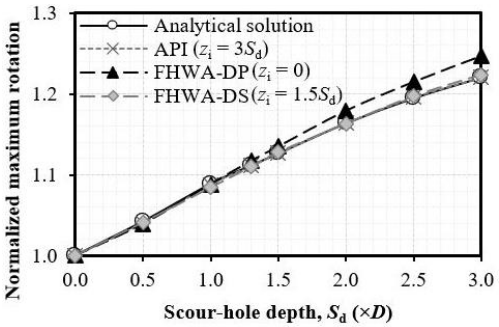


Figure 7. Normalized maximum rotation of pile at post-scour seabed varied by scour-hole depth.

## 6 CONCLUSIONS

This study numerically investigated the dynamic responses of monopile in liquefiable sands under the combined effects of local scour and earthquake using the proposed analytical solution and standard methods (API, FHWA-DP, and FHWA-DS). Based on the analysis results, the following conclusions are drawn:

(1) The maximum bending moment of the pile decreased by 26% as $S_d$ increased from 0 to $2.0D$. Therefore, adopting an overestimated $S_d$ value could underestimate the maximum bending moment of the pile in the post-scour design analysis for a soil-pile-superstructure system with similar dynamic characteristics as the study case. The location of the maximum bending moment moved downward relative to the pile top as $S_d$ increased, which implies that the reinforcement length of the pile shall be extended to a depth of $1.5D$-$3.9D$ below the pre-scour seabed when $S_d = 0$-$3.0D$.

(2) The maximum rotation of the pile at the post-scour seabed increased as $S_d$ increased. A greater value of $S_d$ within the typical design range of $1.3D$-$2.5D$ (e.g., $2.5D$ ) could be employed in the design analysis to provide a more conservative estimation for the rotation response.

(3) Among the three standard methods, API and FHWA-DS rendered agreeable results with the analytical solution. FHWA-DP could cause an unconservative design since it underestimated the scour-induced decrease in the maximum bending moment of the pile.

## 7 ACKNOWLEDGEMENTS

The authors would like to acknowledge the Natural Sciences and Engineering Research Council of Canada (NSERC) for supporting this study through the NSERC Discovery Grant.

## 8 REFERENCES

API. 2011. API RP 2GEO: recommended practice, geotechnical and foundation design considerations. *American Petroleum Institute (API)*, Washington, D.C., USA.

Bhattacharya, S. 2019. Design of foundations for offshore wind turbines. In 1st edition. *John Wiley & Sons Ltd*, West Sussex, UK.

Boulanger, R.W., Curras, C.J., Bruce, B.L., Wilson, D.W., and Abghari, A. 1999. Seismic soil-pile-structure interaction experiments and analyses. *Journal of Geotechnical and Geoenvironmental Engineering*, 125(9): 750–759.

Brandenberg, S.J., Zhao, M., Boulanger, R.W., and Wilson, D.W. 2013. p-y plasticity model for nonlinear dynamic analysis of piles in liquefiable soil. *Journal of Geotechnical and Geoenvironmental Engineering*, 139(8): 1262–1274.

Brown, D.A., Turner, J.P., and Castelli, R.J. 2010. Drilled shafts: construction procedures and LRFD design methods. Technical report, *Federal Highway Administration*, *U.S. Department of Transportation*, Washington, D.C., USA.

Butch, G.K. 1996. Scour-hole dimensions at selected bridge piers in New

York. *American Society of Civil Engineers (ASCE)*, Anaheim, California, USA.
Chang, D., Boulanger, R., Brandenberg, S., and Kutter, B. 2013. FEM analysis of dynamic soil-pile-structure interaction in liquefied and laterally spreading ground. *Earthquake Spectra*, 29(3): 733–755.
DNV. 2014. Design of offshore wind turbine structures. *Det Norske Veritas (DNV)*, Oslo, Norway.
George, G., and Dobry, R. 1984. Simple radiation damping model for piles and footings. *Journal of Engineering Mechanics*, 110(6): 937–956.
Ghosn, M., Moses, F., and Wang, J. 2003. National cooperative highway research program (NCHRP) report 489: design of highway bridges for extreme events. *Transportation Research Board*, Washington, D.C., USA.
GL. 2012. Guideline for the certification of offshore wind turbines. *Germanischer Lloyd (GL) Renewables Certification*, Hamburg, Germany.
Ilankatharan, M. 2008. Centrifuge modeling for soil-pile-bridge systems with numerical simulations accounting for soil-container-shaker interaction. Ph.D. thesis, *University of California, Davis*, Davis, California, USA.
Jia, N., Ding, H., Zhang, P., and Liu, J. 2017. The seismic response of composite bucket foundation for offshore wind turbines under scour conditions. *Proc. 27th International Ocean and Polar Engineering Conference*, San Francisco, California, USA.
Jiang, W., and Lin, C. 2020. Seismic responses of monopile in sands under scour conditions. *Proc. GeoVirtual 2020 Resilience and Innovation Conference*, Canada.
Jiang, W., Lin, C., and Sun, M. 2021. Seismic responses of monopile-supported offshore wind turbines in soft clays under scoured conditions. *Soil Dynamics and Earthquake Engineering*, 142: 106549.
Joyner, W.B., and Chen, A.T.F. 1975. Calculation of nonlinear ground response in earthquakes. *Bulletin of the Seismological Society of America*, 65(5): 1315–1336.
Kampitsis, A.E., Sapountzakis, E.J., Giannakos, S.K., and Gerolymos, N.A. 2013. Seismic soil–pile–structure kinematic and inertial interaction—a new beam approach. *Soil Dynamics and Earthquake Engineering*, 55: 211–224.
Khosravifar, A., Boulanger, R.W., and Kunnath, S.K. 2014. Effects of liquefaction on inelastic demands on extended pile shafts. *Earthquake Spectra*, 30(4): 1749–1773.
Liang, F., Liang, X., Zhang, H., and Wang, C. 2020. Seismic response from centrifuge model tests of a scoured bridge with a pile-group foundation. *Journal of Bridge Engineering*, 25(8): 04020054.
Lin, C., and Jiang, W. 2019. Evaluation of vertical effective stress and pile tension capacity in sands considering scour-hole dimensions. *Computers and Geotechnics*, 105: 94–98.
Lin, C., and Wu, R. 2018. Evaluation of vertical effective stress and pile lateral capacities considering scour-hole dimensions. *Canadian Geotechnical Journal*, 56(1): 135–143.
Lin, Y., and Lin, C. 2019. Effects of scour-hole dimensions on lateral behavior of piles in sands. *Computers and Geotechnics*, 111: 30–41.
Lombardi, D., and Bhattacharya, S. 2016. Evaluation of seismic performance of pile-supported models in liquefiable soils. *Earthquake Engineering & Structural Dynamics*, 45(6): 1019–1038.
Lysmer, J., and Kuhlemeyer, R.L. 1969. Finite dynamic model for infinite media. *Journal of the Engineering Mechanics Division*, 95(4): 859–878.
McKenna, F. 2011. OpenSees: a framework for earthquake engineering simulation. *Computing in Science Engineering*, 13(4): 58–66.
Mo, R., Kang, H., Li, M., and Zhao, X. 2017. Seismic fragility analysis of monopile offshore wind turbines under different operational conditions. *Energies*, 10(7): 1037.
Mosher, R.L. 1984. Load-transfer criteria for numerical analysis of axially loaded piles in sand. Part I: load-transfer criteria. Technical report, *U.S. Army Engineer Waterways Experiment Station*, Vicksburg, MS, USA.
NRCC. 2015. National building code of Canada 2015. *National Research Council of Canada (NRCC)*, Ottawa, Canada.
Patrick, J.H., Frank, R., Garland, E.L., Brent, R.R., and Matthew, L.B. 2016. Design and construction of driven pile foundations. Final report, *Federal Highway Administration, U.S. Department of Transportation*, Washington, D.C., USA.
Seed, H.B., Wong, R.T., Idriss, I.M., and Tokimatsu, K. 1986. Moduli and damping factors for dynamic analyses of cohesionless soils. *Journal of Geotechnical Engineering*, 112(11): 1016–1032.
Tokimatsu, K., Suzuki, H., and Sato, M. 2005. Effects of inertial and kinematic interaction on seismic behavior of pile with embedded foundation. *Soil Dynamics and Earthquake Engineering*, 25(7): 753–762.
Tseng, W.C., Kuo, Y.S., Lu, K.C., Chen, J.W., Chung, C.F., and Chen, R.C. 2018. Effect of scour on the natural frequency responses of the meteorological mast in the Taiwan Strait. *Energies*, 11(4): 823.
Uthayakumar, M., and Naesgaard, E. 2004. Ground response analysis for seismic design in Fraser River Delta, British Columbia. *Proc. 13th World Conference on Earthquake Engineering*, Vancouver, B.C., Canada.
Vijayvergiya, V.N. 1977. Load-movement characteristics of piles. *Proc. 4th Annual Symposium of the American Society of Civil Engineers, Waterway, Port, Coastal and Ocean Division*, CA, USA. 269–284.
Wang, S., Kutter, B.L., Chacko, M.J., Wilson, D.W., Boulanger, R.W., and Abghari, A. 1998. Nonlinear seismic soil-pile structure interaction. *Earthquake Spectra*, 14(2): 377–396.
Whitehouse, R. 1998. Scour at marine structures: a manual for practical applications. In 1st edition. *Thomas Telford Publications*, London, UK.
Yang, Y., Bashir, M., Li, C., and Wang, J. 2019. Analysis of seismic behaviour of an offshore wind turbine with a flexible foundation. *Ocean Engineering*, 178: 215–228.
Yang, Z., Elgamal, A., and Parra, E. 2003. Computational model for cyclic mobility and associated shear deformation. *Journal of Geotechnical and Geoenvironmental Engineering*, 129(12): 1119–1127.
Zhu, B., Wu, X., Wang, Y., and Chen, Y. 2020. Centrifuge modeling for seismic response of fixed-end model piles considering local scour. *Journal of Waterway, Port, Coastal, and Ocean Engineering*, 146(6): 04020041.